Thickness measurement of multilayer film stack in perovskite solar cell using spectroscopic ellipsometry

Cite as: AIP Advances 9, 125107 (2019); doi: 10.1063/1.5125686
Submitted: 25 August 2019 • Accepted: 6 November 2019 •
Published Online: 9 December 2019

Mehedhi Hasan,[1,a)] Kevin Lyon,[2] Lauren Trombley,[2] Casey Smith,[3] and Alex Zakhidov[1,2]

AFFILIATIONS

[1]Materials Science Engineering and Commercialization, Texas State University, San Marcos, Texas 78666, USA
[2]Department of Physics, Texas State University, San Marcos, Texas 78666, USA
[3]Shared Research Operations, Texas State University, San Marcos, Texas 78666, USA

[a)]Author to whom correspondence should be addressed: mehedhi.hasan@txstate.edu

ABSTRACT

The rapid surge in perovskite solar cell efficiency has necessitated the development of viable metrology techniques during device integration, paving the way for commercialization. Ellipsometry is considered the most appropriate technique for fast and accurate thickness measurement for large scale production. However, a precise and well-calibrated model is a prerequisite for this technique. While ellipsometry of individual device layers has been reported in recent perovskite literature, a comprehensive multilayer modeling approach is thus far unavailable. Perovskite optoelectronic devices generally consist of a six-layer film stack with three transparent layers required for optical absorption in the perovskite layer. Spin casted thin films, now common in this line of research, impart their own difficulties into ellipsometric modeling. Roughnesses at each heterointerface, similarities in optical spectra of transparent layers, and anomalous dispersion of perovskite are just a few of such challenges. In this work, we report the process of building an ellipsometry model from scratch for thickness measurement of methylammonium lead iodide (MAPI) perovskite and indium tin oxide (ITO)/hole transport layer (HTL) bilayer thin film stacks on a glass substrate. Three promising representatives of HTLs (CuI, Cu_2O, and PEDOT:PSS) were studied. The models were extended to measure the individual layer thicknesses of the MAPI/HTL/ITO film stack on a glass substrate using the models developed for individual layers. Optical constants of all the representative thin films were thus extracted for a wide wavelength range (300 nm–900 nm).

After remarkable successes at laboratory scale, efforts for making commercialized hybrid perovskite solar cells are underway.[1,2] Perovskite solar cells are generally six-layer film stacks arranged as shown in Fig. 1(a).[3] Most of the layers can be easily deposited using solution-based spin coating, which makes these devices a very promising and low-cost alternative to current commercial solar cells. The worldwide effort in perovskite research has been mainly focused on the stability challenges of organic perovskites, leaving the issue of developing commercially viable metrology processes largely unaddressed.[4] Metrology is an integral part of both commercial production and research for reproducibility and quality assurance. Particularly, the optimum thickness of individual layers is crucial for overall device performance. Many different techniques have historically been employed for thin film thickness measurements such as stylus profilometry, spectroscopic ellipsometry (SE), X-ray reflectivity (XRR), atomic force microscopy (AFM), film thickness reflectometry, and scanning electron microscopy (SEM).[5,6] All these techniques have relative advantages and disadvantages.

An ideal metrology technique must be fast, accurate, nondestructive, repeatable, and robust and should not require any sample preparation. SE fulfills all the criteria, provided that accurate models are available. It is already widely adopted in high volume manufacturing for thickness measurements as well as investigating optical properties.[7] In addition, film roughness, material composition, and doping concentration can be derived from ellipsometry data. Modeling of a smooth surface single layer thin film on a standard substrate

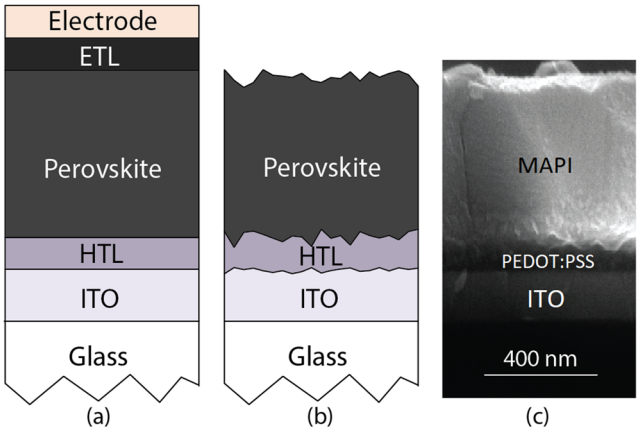

FIG. 1. (a) Inverted planar solar cell architecture with ideal interfaces. (b) Schematic model of MAPI/HTL/ITO on glass substrate with interfacial roughness and intermixing shown. (c) Cross-sectional SEM image of fabricated MAPI/PEDOT:PSS/ITO stack on glass substrate.

(such as silicon or glass) for known properties is straightforward. However, real methylammonium lead iodide (MAPI) solar cells have rough interfaces between constituent layers. In this work, we model the three bottom layers of a MAPI solar cell. Figures 1(b) and 1(c) illustrate the schematic model and SEM cross sectional image, respectively, of a MAPI/hole transport layer (HTL)/indium tin oxide (ITO) film stack on glass. Note that the interfaces are not abrupt in real samples, which can complicate modeling efforts. Modeling of multilayer film stacks is also complicated for several other reasons. First, the number of unknown parameters increases with each added layer. Second, reflection from multiple interfaces causes many peaks and valleys to form in the SE spectra because of constructive and destructive interference. Finally, back reflection and optical similarities between transparent layers can make individual layer modeling difficult.[8,9]

The goal of this research is to develop a model for a perovskite based solar cell stack, as in Fig. 1(c), although the general procedure detailed in this work can be applied to other film stacks. A wide verity of hybrid perovskite with ABX_3 general formula, where A represents an organic cation such as methylammonium ($CH_3NH_3^+$) ion or formamidinium ($CHNH_3^+$) ion, B represents a metal ion (e.g., Pb_2^+, Sn_2^+, or Cd_2^+), and X denotes a halogen ion (e.g., I^-, Br^-, or Cl^-), have been utilized as solar cell absorber.[10,11] From the literature study, it has been observed that most of the large area devices were based on methylammonium lead iodide (MAPI) perovskite.[12] Presuming the prospect of commercialization, MAPI is considered as representative of perovskite. Moreover, the optical properties of MAPI are widely available in literature for comparison. There are two categories of HTL, organic and inorganic. Spiro-OMeTED, PEDOT:PSS, PTA, and P3HT are the popular representatives of organic HTL.[13] On the other hand, CuI, Cu_2O, NiO_x, and MoO_x are reported as inorganic HTL.[11] Taking the energy level matching with MAPI into account, we selected the HTLs that represent both organic (PEDOT:PSS) and inorganic (CuI, Cu_2O) thin films. Among the inorganic HTLs, CuI is represented as single phase and Cu_2O is represented as amorphous.

Optical modeling and dispersion properties were investigated by ellipsometry for MAPI,[14] $MAPbI_{3-x}Cl_x$,[9] $Cs_yFA_{1-y}Pb(I_xBr_{1-x})_3$,[15] and $FAPbI_xBr_{3-x}$[16] perovskite species. In particular, the benchmark perovskite MAPI was extensively studied for complex refractive index (n) spectra[14] and optical transitions[17,18] using SE and results verified with theoretical calculations. In most cases, only the individual MAPI layer was taken into consideration. Reports are also available on $MAPbI_{3-x}Cl_x$/PEDOT:PSS/ITO film stacks to explore optical properties and aid tandem solar cell design. Optical data obtained from SE have been reported for PEDOT:PSS,[19] CuI,[20,21] and Cu_2O[22] thin films. Published SE results for PEDOT:PSS were focused on conductivity changes from various types of doping.[23,24] For γ-CuI deposited via acetonitrile solution spin coating, absorbance and transmission spectra obtained from the dielectric function measured by SE have been reported,[20] though the specifics of the optical model fitting are only superficially stated. Similarly, other literature has reported on the ellipsometric parameters, Ψ and Δ, of a γ-CuI thin film deposited by reactive DC-sputtering and its relation to the dielectric function.[21] However, this source does not expound further on the connection between the numerical model used and the measured optical parameters. Literature for Cu_2O has been more thorough in describing the ellipsometric models used for fitting as well as their specific connection to the measured quantities such as absorption, n, bandgap, and dielectric constant.[22,25,26] However, these sources report on crystalline Cu_2O deposited by a variety of techniques other than the spin coating used in this work, which resulted in amorphous Cu_2O. While these data are useful for comparing material samples to known measurement values, a process for generating a reliable ellipsometry model for these materials, as well as how these models correspond to the measured quantities, is lacking in current literature.

Each of the listed HTLs are transparent and expected to have high optical similarities with ITO and glass. Quantification of correlation in dispersion properties of optically similar film stacks is essential for design consideration as well as optical metrology. This work is intended to close these gaps and includes SE analysis of both inorganic and organic polymer based HTLs with crystalline and amorphous morphologies. This work also seeks to develop a consistent procedure for building a working SE model for bilayer and trilayer heterojunction architectures that include several transparent layers.

Individual thin films and thin film stacks of best possible quality were deposited on glass substrates or ITO/glass substrates as required. The thickness of the films was varied either by changing the spin speed or the solution concentration. The detailed process of thin film deposition procedures is described in the supplementary material.

The J. A. Wollam M2000 ellipsometer was used for collecting SE spectra, and CompleteEASE software was used for analysis and modeling. For profilometer thickness measurements, multiple profiles were taken using a Bruker DektakXT at different locations on each sample, so that a reliable average thickness could be calculated. SEM images were taken on the FEI Helios NanoLab 400 DualBeam field emission scanning electron microscope. The Bruker Dimension ICON atomic force microscope was used for AFM imaging and step height measurement. A Rigaku SmartLab diffractometer was used for collecting XRD data.

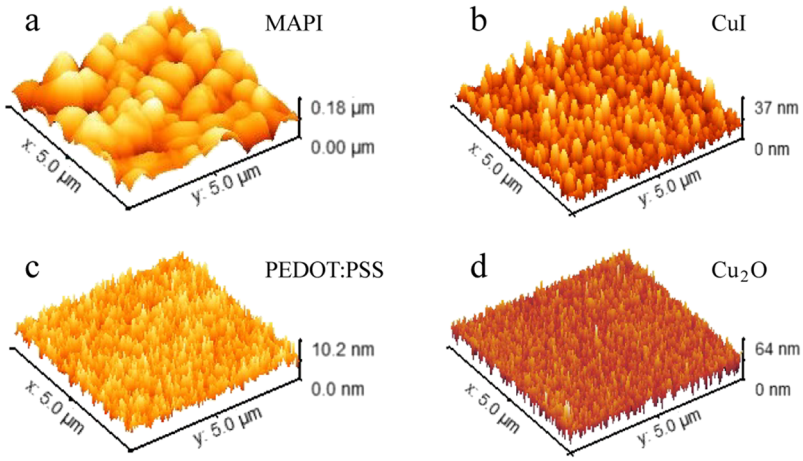

FIG. 2. AFM image of (a) MAPI, (b) CuI, (c) PEDOT:PSS, and (d) Cu_2O.

To aid in the construction of models for each material, thickness data from profilometry and roughness data from AFM were incorporated. The thickness of MAPI films ranged from 125 to 350 nm and that of HTLs ranged from 15 to 65 nm, which is within the typical range required for solar cell devices. AMF images of the MAPI and HTLs films are shown in Figs. 2(a)–2(d). MAPI and CuI had a granular surface morphology with comparatively high roughness. On the other hand, no granular pattern was observed for PEDOT:PSS or Cu_2O film surfaces. The root mean squared (rms) roughness of 5 μm × 5 μm area of the selected MAPI, CuI, PEDOT:PSS, and Cu_2O films was 23 nm, 5.3 nm, 1.2 nm, and 7 nm, respectively. MAPI thin film was polycrystalline whereas the CuI film was single phase confirmed by XRD study as shown in the supplementary material Fig. S1. Both PEDOT:PSS and Cu_2O were amorphous.

Along with this supplementary material, selection of an appropriate analysis model requires knowledge of the absorption or transmission spectra of the film. For this, ultraviolet-visible (UV-Vis) spectroscopy was performed on all films. MAPI exhibited highly absorptive behavior via UV-Vis, while HTLs and substrate materials were highly transparent in the visible range as expected [Fig. 3(b)]. Absorption started toward the UV range, with different onset wavelengths for different HTLs. The modeling procedure for MAPI, HTLs, and ITO layers are now discussed separately for convenience.

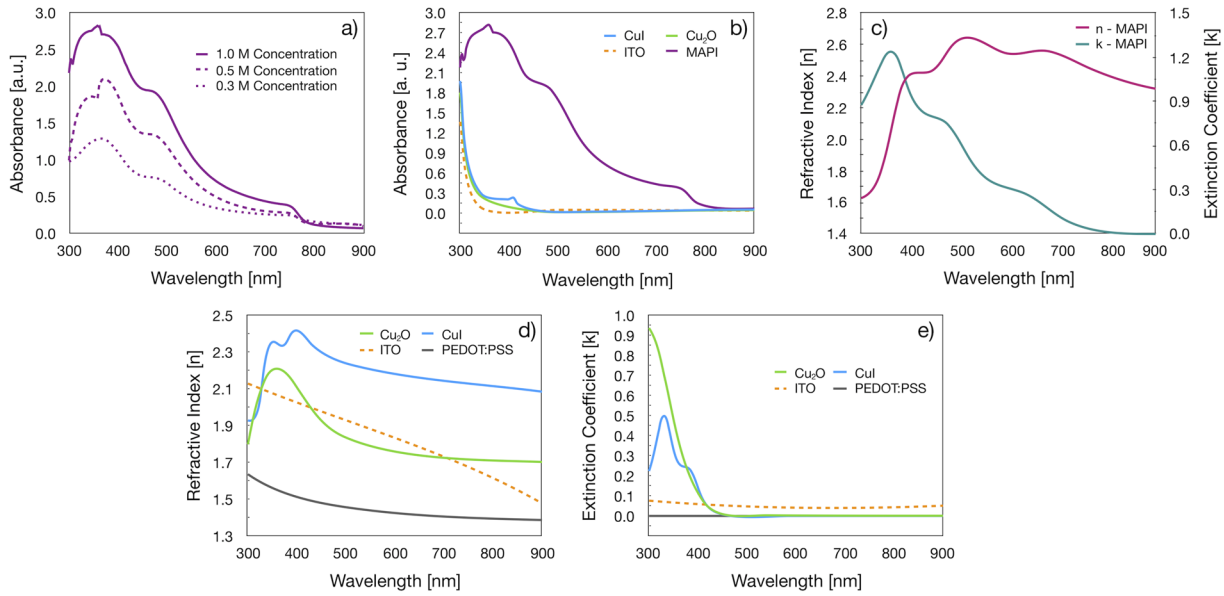

FIG. 3. (a) UV-Vis absorption spectra of MAPI thin film for various thickness. Different film thicknesses were achieved by changing the concentration of precursor solution. (b) UV-Vis absorption spectra of MAPI, CuI, Cu_2O, PEDOT:PSS, and ITO thin films. (c) *n* and *k* of MAPI thin film determined by global fitting of B-spline method, (d) *n* for all HTLs and ITO, and (e) *k* for all HTLs and ITO.

As can be seen in Fig. 3(a), MAPI films have high absorbance over the entire visible range (390–780 nm). The onset of absorption is at 780 nm, which implies a bandgap of ~1.58 eV. Two other absorption peaks are observed at 375 nm (3.3 eV) and 480 nm (2.58 eV). While absorption was higher for thicker films, the shape of the absorption spectra was similar regardless of thickness. B-spline is the recommended method in CompleEASE for partially or fully absorptive materials as it allows arbitrary flexibility of n and the extinction coefficient (k) over the entire spectra. For MAPI, B-spline was selected as the initial model. The thickness from profilometer (~335 nm) and root mean squared (rms) roughness from AFM (~23 nm) were used as fixed input parameters. We then performed global fitting over a range of n and k values with a defined number of steps. The best fit was obtained for n and k ranging from 1.3 to 3.0 and 0.0 to 1.5, respectively. The estimated n and k spectra for MAPI thin films are shown in Fig. 3(c), which agree closely with the reported spectra.[14] Several verification steps were applied to assess the validity and accuracy of optical constants. First, the k spectra from the model is expected to be similar to the measured absorption spectra from UV-Vis. From Figs. 3(a) and 3(c), the absorption peaks conform with the modeled k. The values of n and k are also physically meaningful,

$$MSE = \sqrt{\frac{1}{3m-l}\sum_{i=1}^{m}\left[\left(N_{E_i}-N_{G_i}\right)^2+\left(C_{E_i}-C_{G_i}\right)^2+\left(S_{E_i}-S_{G_i}\right)^2\right]}\times 1000. \quad (1)$$

To quantify the accuracy of the model, a goodness-of-fit parameter, mean squared error (MSE), was used as defined in Eq. (1), where m is the number of wavelengths sampled, l is the number of fitted parameters, and measurement vectors $N = \cos(2\Psi)$, $C = \sin(2\Psi)\cos(\Delta)$, and $S = \sin(2\Psi)\sin(\Delta)$ are added in quadrature after quantifying the difference between a model generated value, G, and the experimentally measured value, E.[7,24,27] Performing a global fit for each measurement is a time consuming exercise, especially when the step size of parameters is small. Moreover, we can end up with misleading results caused by process drift as global fit can alter n and k to reduce MSE. Thus, it is a useful tool for optimization, but not a proper choice for final modeling.

To build a straightforward model for quick measurements, the model was rebuilt by parameterizing optical constants using a general oscillator (GEN-OSC) approach. In this step, the optical constants obtained from B-spline global fit were modeled as a sum of Tauc-Lorentz oscillators. Each such oscillator is defined by an energy center, amplitude, broadening, and bandgap parameter. Energy centers are associated with interband transitions, where the amplitude determines the strength of peak. The shape of the individual oscillator can be constructed by a broadening parameter. Different energy centers contribute differently during light material interaction that can be found in absorption spectra. By adjusting the oscillator parameters, the complicated optical properties can be formulated as sum of oscillators. From the k spectra, three absorption peaks were observed at ~2.0 eV, ~2.5 eV, and ~3.3 eV. Two of these peaks matched closely with UV-Vis measurements. The absorption peak at 2.0 eV was not distinguishable via UV-Vis. Each energy center mentioned is associated with a valance-to-conduction band transition confirmed by experiment and theoretical study.[15] The bandgap was calculated to be ~1.58 eV and ~1.56 eV from UV-Vis and SE, respectively, which agrees with literature.[15] To construct the model, the sum of three oscillators was used, with energy centers located at known absorption peaks. The amplitude and broadening parameters were adjusted for best fit. Two additional oscillators were required to fit the nonzero absorption tail above 4.0 eV. All specific oscillator parameters assigned for best fit are listed in Table SI of the supplementary material.

After finalizing the models, it was applied to estimate thicknesses of three different samples. These estimates were validated using a profilometer in three different locations. Both types of models measure film thicknesses accurately below 200 nm, with reasonable accuracy (deviation ≤5%) for thicker samples. It is observed that, for higher thicknesses, MSE and deviation between measurements increased. One of the sample thickness was measured by SEM cross section and AFM step height measurement. All thickness results can be seen summarized in Table SII of the supplementary material.

UV-Vis absorption data show that CuI, Cu_2O, PEDOT:PSS, and ITO layers are optically transparent over the range 450–900 nm, with absorption onsets all below 450 nm [Fig. 3(b)]. Optical transparency in the visible spectrum allows for us to assume that $k = 0$ over this range. With this condition, n can be described as a function of wavelength, λ, using a Cauchy equation in Eq. (2) to three terms. Coefficients a, b, and c can then be optimized by CompleteEASE software,

$$n(\lambda) = a + \frac{b}{\lambda^2} + \frac{c}{\lambda^4} + \cdots. \quad (2)$$

To build a model for the entire UV-Vis spectrum (300–900 nm), the procedure was done in two strategic spectral regimes. In the first segment (450–900 nm), known thickness and roughness values were provided, k was set to zero, and the Cauchy coefficients were optimized by a nonlinear fitting procedure until best fitting values were found for this range. MSEs of these results were then used to determine goodness-of-fit. The values for n at 632.8 nm (monochromatic red) found by the Cauchy method were 2.19 for CuI, 1.75 for Cu_2O, and 1.42 for PEDOT:PSS. In the second segment, the value of k in the spectral range of 300–450 nm can neither be constant nor zero. This suggests B-spline as the proper method to find k. Thus, n and k for CuI and Cu_2O were extracted following the same procedure as MAPI. The n values obtained by the Cauchy method were supplied as a starting parameter along with thickness and roughness. Then, the final n and k values over both wavelength regimes were combined to fill the entire UV-Vis range. Finally, to complete the model, n and k were parameterized

as the sum of three oscillators with similar procedures to MAPI modeling. Oscillator parameters are seen in Table SI of the supplementary material. The bandgap determined for the best fit CuI and Cu_2O oscillator model was 2.9 eV and 2.7 eV, respectively. The reported bandgap of crystalline CuI and Cu_2O are 3.1 eV and 2.7 eV, respectively.[21,28] Moreover, the energy centers selected for Tauc-Lorentz oscillators for CuI shows good agreement with the peak of dielectric function reported in Ref. 21. For PEDOT:PSS, Cauchy coefficients were optimized as a = 1.196, b = 0.0756, and c = 0.001 23. Different model options were available in the CompleteEASE library for ITO. Since the optical properties of ITO films differ from process to process, a parameterized ITO model was selected and modified to match the ITO properties for this research. Finding ITO thickness was not required for this work since ITO/glass substrates came from vendors with a known thickness of 110 nm. However, the ITO model was still essential for bi-/trilayer modeling. The accuracy of the ITO model was validated by comparing measured thickness via a profilometer. The n and k values for all HTLs and ITO are shown in Figs. 3(d) and 3(e), respectively.

The individual optimized models were added sequentially and modified as required to make a single model for use on a HTL/ITO bilayer and MAPI/HTL/ITO trilayer film stack. For accuracy of multilayer modes interface roughness, intermixing, and backside reflection are the crucial issues to consider. We used Bruggeman Effective Medium Approximation (BEMA) at the HTL/ITO and MAPI/HTL interfaces. However, the introduction of a BEMA layer compromised the MSE as well as measured thicknesses. This may be attributed to the increased number of variables for the additional layer(s). Note that the roughness of MAPI is significantly higher than that of other layers. Thus, in bilayer and trilayer models, the introduction of the top layer roughness only resulted in acceptable accuracy instead of using BEMA at each interface. To suppress the backside reflection from the transparent sublayers, the common practice is to roughen the bottom surface by various methods.[29] We used the "backside reflection" fit parameter in the analysis software to avoid additional processing on the sample. After constructing bilayer models for each HTL/ITO, we utilized them for the measurement of samples with varied thicknesses. To investigate the impact of optical correlation between the HTL and ITO, we utilized two versions of the bilayer model. One version had the ITO thickness fixed (110 nm) while the HTL thickness was fitted. The other version had both layer thicknesses fitted. While the CuI/ITO model estimated thicknesses of both layers individually with high accuracy, the PEDOT:PSS/ITO and Cu_2O/ITO models only estimated the thickness of the HTL accurately when the ITO thickness was fixed. In the case where both thicknesses were allowed to fit, the total thicknesses were estimated with high accuracy at the expense of individual thickness accuracy. Still, the models proved generally useful since ITO/glass substrates with known ITO thickness is commonplace. All these results can be seen in Table SIII of the supplementary material. The inability of these bilayer models to resolve the thicknesses of PEDOT:PSS, Cu_2O, and ITO individually was attributed to the high optical dispersion correlation between the HTL and the ITO layer. The correlation of the CuI/ITO, Cu_2O/ITO, and PEDOT:PSS/ITO bilayers are 53.9%, 97.5%, and 83.0%, respectively. Thus, a higher deviation in estimated thickness was observed for a higher optical correlation. This result, then, is not as much a limitation of the model as it is a limitation caused by fundamental material properties. As such, knowing the optical dispersion correlation between bilayer materials is important to consider when building SE models.

Adding another layer sequentially as above, we further extended the model to estimate thicknesses of a trilayer film stack. For a trilayer representative, a MAPI/PEDOT:PSS/ITO model was constructed. From this model, the thicknesses of each layer could not be resolved individually for the same reason as described before. However, using the strategy of bilayer measurement, if we already know the thicknesses of the HTL/ITO stack, those can be used as input for the trilayer measurement. Then, the third layer (MAPI) thickness can be estimated via fitting with reasonably high accuracy. These results can be seen in Table SIV of the supplementary material.

In summary, we developed a consistent procedure for building a working SE model for bilayer and/or trilayer heterojunction material stacks that consist of multiple transparent layers. This methodology should also be applicable for other hole and electron transport materials applied to organic lead halide perovskite solar cells. Once established, these models should allow for fast and repeatable ellipsometry characterization of these photovoltaic devices, including the thicknesses and optical properties of constituent layers. Knowing the value of optical constants will play a role in selection and designing more effective optoelectronic device architectures and tandem solar cells.

See the supplementary material for the detailed sample preparation, XRD data of the thin films, general oscillator parameters values of the models, and thickness data measured by using a profilometer and estimated by using an ellipsometer.

This research was supported by NSF SBIR (Grant No. 1721884, Program Manager Dr. Anna Brady-Estevez), ACS Petroleum Research Fund (Grant No. UNI656095-UNI6, Program Manager Dr. Askar Fahr), and Office of Naval Research HBCU/MI instrumentation (Grant No. W911NF-16-1-0518, Program Manager Dr. Paul Armistead).

REFERENCES

[1] L. Qiu, L. K. Ono, and Y. Qi, Mater. Today Energy **7**, 169 (2018).
[2] Y. Rong, Y. Hu, A. Mei, H. Tan, M. I. Saidaminov, S. Il Seok, M. D. McGehee, E. H. Sargent, and H. Han, Science **361**, eaat8235 (2018).
[3] S. Venkatesan, M. Hasan, J. Kim, N. R. Rady, S. Sohal, E. Neier, Y. Yao, and A. Zakhidov, J. Mater. Chem. C **5**, 10114 (2017).
[4] Q. Fu, X. Tang, B. Huang, T. Hu, L. Tan, L. Chen, and Y. Chen, Adv. Sci. **5**, 1700387 (2018).
[5] P. Whiteside, J. Chininis, and H. Hunt, Coatings **6**, 35 (2016).
[6] A. Piegari and E. Masetti, Thin Solid Films **124**, 249 (1985).
[7] C. Yim, M. O'Brien, N. McEvoy, S. Winters, I. Mirza, J. G. Lunney, and G. S. Duesberg, Appl. Phys. Lett. **104**, 103114 (2014).
[8] J. N. Hilfiker, G. K. Pribil, R. Synowicki, A. C. Martin, and J. S. Hale, Surf. Coat. Technol. **357**, 114 (2019).
[9] C. W. Chen, S. Y. Hsiao, C. Y. Chen, H. W. Kang, Z. Y. Huang, and H. W. Lin, J. Mater. Chem. A **3**, 9152 (2015).
[10] Q. Chen, N. De Marco, Y. Yang, T. Bin Song, C. C. Chen, H. Zhao, Z. Hong, H. Zhou, and Y. Yang, Nano Today **10**, 355 (2015).
[11] P. K. Kung, M. H. Li, P. Y. Lin, Y. H. Chiang, C. R. Chan, T. F. Guo, and P. Chen, Adv. Mater. Interfaces **5**, 1800882 (2018).

[12]Y. Chen, L. Zhang, Y. Zhang, H. Gao, and H. Yan, RSC Adv. **8**, 10489 (2018).
[13]S. Pitchaiya, M. Natarajan, A. Santhanam, V. Asokan, A. Yuvapragasam, V. M. Ramakrishnan, S. E. Palanisamy, S. Sundaram, and D. Velauthapillai, "A review on the classification of organic/inorganic/carbonaceous hole transporting materials for perovskite solar cell application," Arab. J. Chem. (published online).
[14]M. Stuckelberger, B. Niesen, M. Filipic, S. Moon, J. Yum, M. Topic, S. De Wolf, and C. Ballif, J. Phys. Chem. Lett. **6**, 66–71 (2015).
[15]J. Werner, G. Nogay, F. Sahli, T. C. J. Yang, M. Bräuninger, G. Christmann, A. Walter, B. A. Kamino, P. Fiala, P. Löper, S. Nicolay, Q. Jeangros, B. Niesen, and C. Ballif, ACS Energy Lett. **3**, 742 (2018).
[16]H. Shirai, in *Ellipsometry: Principles and Techniques for Materials*, 1st ed., edited by F. Wahaia (IntechOpen, 2017), pp. 91–106.
[17]M. Shirayama, H. Kadowaki, T. Miyadera, T. Sugita, M. Tamakoshi, M. Kato, T. Fujiseki, D. Murata, S. Hara, T. N. Murakami, S. Fujimoto, M. Chikamatsu, and H. Fujiwara, Phys. Rev. Appl. **5**, 014012 (2016).
[18]A. M. A. Leguy, P. Azarhoosh, M. I. Alonso, M. Campoy-Quiles, O. J. Weber, J. Yao, D. Bryant, M. T. Weller, J. Nelson, A. Walsh, M. van Schilfgaarde, and P. R. F. Barnes, Nanoscale **8**, 6317 (2016).
[19]J. Weszka, M. M. Szindler, and P. Jarka, J. Achiev. Mater. Manuf. Eng. **59**, 59–66 (2013).
[20]S. A. Mohamed, J. Gasiorowski, K. Hingerl, D. R. T. Zahn, M. C. Scharber, S. S. A. Obayya, M. K. El-Mansy, N. S. Sariciftci, D. A. M. Egbe, and P. Stadler, Sol. Energy Mater. Sol. Cells **143**, 369 (2015).
[21]E. Krüger, V. Zviagin, C. Yang, C. Sturm, R. Schmidt-Grund, and M. Grundmann, Appl. Phys. Lett. **113**, 172102 (2018).
[22]H. Derin and K. Kantarli, Appl. Phys. A: Mater. Sci. Process. **75**, 391 (2002).
[23]J. Gasiorowski, R. Menon, K. Hingerl, M. Dachev, and N. S. Sariciftci, Thin Solid Films **536**, 211 (2013).
[24]T. Syrovy, P. Janicek, J. Mistrik, K. Palka, P. Hawlova, L. Kubac, and M. K. Gunde, Synth. Met. **227**, 139 (2017).
[25]R. A. Powell, D. Settles, L. Lane, C. L. Ygartua, A. R. Srivatsa, and C. Hayzelden, in *Process Control Diagnostics* (SPIE, 2003), Vol. 4182, p. 97.
[26]N. Mårtensson, "Optical properties of silica-copper oxide thin films prepared by spin coating," Ph.D. dissertation (Linköping University, 2011).
[27]M. Mazumder, R. Ahmed, M. Hasan, M. Lee, and M. Lee, Int. J. Civ. Eng. **5**, 1–9 (2019).
[28]O. Messaoudi, H. Makhlouf, A. Souissi, I. Ben Assaker, M. Karyaoui, A. Bardaoui, M. Oueslati, and R. Chtourou, J. Alloys Compd. **611**, 142 (2014).
[29]R. A. Synowicki, Phys. Status Solidi C **5**, 1085 (2008).